

Fatigue Behavior Analysis and Multi-Scale Modelling of Chopped Carbon Fiber Chip-Reinforced
Composites under Tension-Tension Loading Condition

Haibin Tang ^{a†}, Zhangxing Chen ^{b†}, Guowei Zhou ^{c†}, Li Huang ^d, Katherine Avery ^d, Yang Li ^d, Haolong Liu ^a, Haiding Guo ^{a*}, Hongtae Kang ^c, Danielle Zeng ^d, Carlos Engler-Pinto ^d, Xuming Su ^d

^a Jiangsu Province Key Laboratory of Aerospace Power System, College of Energy and Power Engineering, Nanjing University of Aeronautics and Astronautics, Nanjing 210016, China

^b State Key Laboratory of Mechanical Transmission, Chongqing University, Chongqing 400044, China

^c College of engineering, Ohio State University Columbus, OH, 43212, USA

^d Research and Innovation Center, Ford Motor Company, Dearborn, MI, 48124, USA

^e College of Engineering and Computer Science, University of Michigan-Dearborn, 4901 Evergreen Road, Dearborn, MI, USA

† These authors contributed equally to this work.

* Corresponding author. Email: ghd@nuaa.edu.cn

Abstract

In present study, the fatigue damage behavior of chopped carbon fiber chip-reinforced composite has been experimentally and numerically investigated. A large scatter is exhibited in the $S-N$ diagram due to the random distribution of carbon fiber chips, and therefore a new analysis procedure is proposed to link the local microstructure to the fatigue behavior of the bulk material. Interrupted fatigue tests are also performed so that microstructure characterization can be conducted on the tested samples to analyze the crack initiation and propagation. Inspired from the experimental findings, a multi-scale progressive damage fatigue model is proposed to predict the fatigue behavior. The model incorporates a new stochastic chip-packing algorithm for microstructure reconstruction along with continuum damage models into the representative volume element (RVE) model in ABAQUS/Explicit. The simulation results based on the proposed model are in good agreement with the experimental data in terms of cracking modes and predicted life.

Keywords: chopped carbon fiber chip-reinforced composite; tension-tension fatigue behavior; crack initiation and propagation; multi-scale fatigue model

Notation

1. $E_{average}$: Average modulus

$E_{average} = \sigma / (\varepsilon_{local} / 2 + \varepsilon_{local-opposing} / 2)$, ε_{local} and $\varepsilon_{local-opposing}$ are the local surface strain of two opposing surfaces for a local area, e.g., 1mm × 25.4mm (longitudinal length × transverse width).

2. E_{RL} : relative low average modulus

$E_{RM} \leq E_{RL} \leq 1.1 * E_{RM}$, E_{RM} is the lowest average modulus within specimen.

1. Introduction

Discontinuous fiber or chip-reinforced composite materials have attracted increasing interest as promising alternatives to aluminum and steel for applications in the automotive industry [1-3]. In particular, chopped carbon fiber chip-reinforced composites, which are produced by a compression molding approach as a sheet molding compound, provide a new material fabrication form for engineers. The chopped carbon fiber chip-reinforced composites show great advantages due to their better balance between mechanical performance and manufacturing costs compared with continuous fiber-reinforced composites [4, 5]. These materials are also more suitable for the manufacture of complex geometrical structures. However, most effort is made on property analysis under the monotonic loading condition. Fatigue failure analysis of chopped carbon fiber chip-reinforced composites is still indispensable for further promotion.

Monotonic tensile failure analysis has already been conducted for several types of chopped carbon fiber chip-reinforced composites. The results indicate that chopped carbon fiber chip-reinforced composites show a heterogeneous property at the macro-scale level owing to the randomly distributed chips. Feraboli et al. [1, 6-8] assess the elastic modulus of the chopped carbon fiber chip-reinforced composite. Significant variations of local modulus in single specimens are observed by strain gage and extensometer as well as by digital image correlation (DIC) measurement. Johanson et al. [9] prove the significant variation in the strain field between two surfaces of chopped carbon fiber chip-reinforced composite during tension after a detailed comparison of the strain field taken immediately prior to failure. On this basis, Tang et al. [10] point out that the failure initiation coincides with a strain localization observable from both sides of the tested samples. The average modulus is a good indicator of tensile failure and can be related to the chip orientation distribution at the failure area. Accordingly,

the prominent heterogeneity should also be incorporated into the tension-tension fatigue analysis for chopped carbon fiber chip-reinforced composites.

In contrast, very limited research work has been conducted on fatigue failure of chopped carbon fiber chip-reinforced composites. Selezneva et al. [11] have evaluated the fatigue performance of chopped carbon fiber chip-reinforced composites under a stress ratio of 0.1. A good correlation between stress range and life is obtained, and no obvious damage is observed away from the failure area. The limited fatigue results in Ref. [11] may mask the effect of material heterogeneity, which has been observed in quasi-static tensile loading [10]. Hence, further investigation is required to get more insight into the related fatigue behavior and failure mechanism.

Due to the limited number of durability analyses of chopped carbon fiber chip-reinforced composites, the following review will focus on short fiber-reinforced composites, which have similar heterogeneous properties. Different monotonic and cyclic behaviors are observed in short fiber reinforced samples cut from different locations, which is induced by various fiber distributions [12, 13]. Accordingly, Horst et al. propose a master curve to describe the effect of fiber distribution on fatigue behavior. The fatigue crack propagation also shows fiber distribution dependence. Tanaka et al. [14] point out that the propagation rate of notched samples is determined by the range of the stress intensity factor divided by the elastic modulus. In comparison, Monte et al. [15-17] claim that the Tsai-Hill failure criterion can be adapted and used in the cyclic loading condition for short fiber-reinforced composites. Based on the previous studies, a combination between these approaches and fatigue characteristics is a potential way to improve the life prediction of chopped carbon fiber chip-reinforced composites.

The aim of the present work is to evaluate the tension-tension fatigue behavior of chopped carbon fiber chip-reinforced composites. The correlation between fatigue failure and local material properties is explored in detail for tension-tension fatigue tests via in-situ DIC. Further, microstructure characterization is performed on the samples at the early stage of the fatigue procedure as well as just prior to the final failure. On this basis, a multi-scale fatigue model is established. Different corresponding continuum damage models are defined for the damage evolution of chip, resin and interface in the modified reconstruction model built with a modified random sequential absorption algorithm. The proposed multi-scale fatigue model is validated by several cases with different chip distributions.

2. Materials and test setup

2.1. Materials

The chopped carbon fiber chip-reinforced SMC plaques (hereinafter “SMC”) are formed by compression molding from the initial charges. The initial charges are made from chopped carbon fiber chips, uncured thermoset resin with a glass transition temperature in excess of 140°C, and curing agent. They are cut into several quadrants and piled up together in a specific order before compression molding. After that, the SMC plaques are formed at specific temperature and press force. The manufacturing process is illustrated in Figure 1, similar to the methodology presented in Ref. [18]. The dimensions of the SMC plaques are 457.2mm × 457.2mm with thicknesses of 4.8mm. The labeled fiber volume fraction of the SMC plaques by the material supplier is 40%. The chips in SMC plaques are random oriented. However, in some local areas, chips may moderately align along some direction and thus deviate from random orientation. The maximum cross-section of the chip is approximately 5mm × 0.1mm and the maximum length is around 25mm.

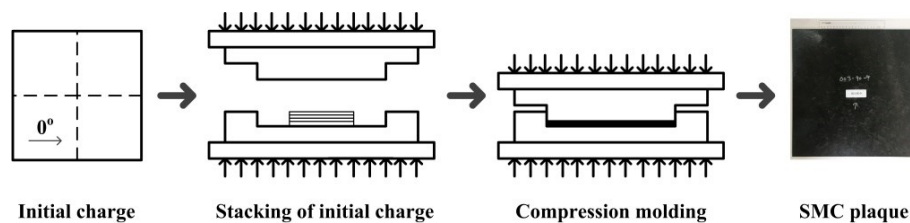


Figure 1. Manufacturing processing of SMC plaques

2.2. Fatigue test setup

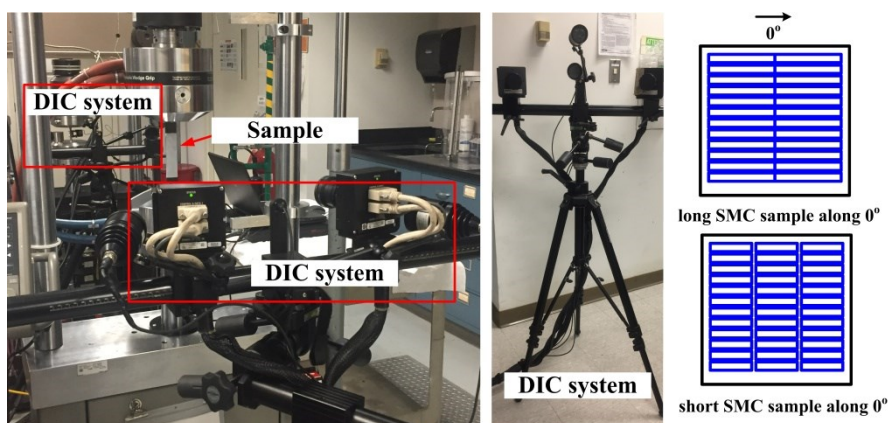
Two types of fatigue samples with different gauge sections, i.e., the long sample and the short sample, are prepared according to ASTM standard D3479 [19], the gauge section of which is 127mm × 25.4mm and 50.8mm × 25.4mm, respectively. Since there are no significant variations of material properties for bars cut along different orientations [10], all samples are prepared along 0°, which is a fixed direction along a consistent edge of the mold for SMC plaques.

Load-controlled fatigue tests are performed using an MTS servo hydraulic frame at 5 Hz with a sinusoidal waveform. The load ratio, which is defined as the minimum load divided by the maximum load in a cycle, is 0.1. During fatigue testing, the temperature at the center of the samples is monitored by a pyrometer (Model RAYMML TSVF1L). The thermal camera (Gobi-640-GigE Industrial) is also

applied for further verification of the temperature increment.

Prior to fatigue testing, each sample is loaded to 100MPa (nominal stress), which is less than half of its tensile strength, to acquire the strain distributions of two opposing sides using two ARAMIS DIC systems, as shown in Figure 2(a). The samples are first coated with a white spray paint, and then a random pattern of black speckle marks is applied to the surface to meet the requirement of the DIC systems. Two ARAMIS DIC systems are aligned by the edge of the painted area on the sample surface, which is strictly controlled to be the same location with the same planar coordinates on both faces. The DIC systems are calibrated by the standard pattern, and the accuracy of strain measurement is verified. In the post-processing of the DIC results, the facet size is set as 15 pixels, which correspond to 1mm on the specimen.

Meanwhile, interrupted fatigue tests are conducted to get insight into the damage mechanism. The fatigue tests are suspended on selected samples, and microstructure characterizations are performed at some potential failure areas. Sequential imaging of the in-plane section of the samples through the thickness direction is enabled by an automatic polishing system (MuitiPrep™ System 15-2000-GI produced, Allied High Tech Products, Inc.), which is able to remove a thin layer of the material from a polished surface. An example of images is shown in Figure 2(b). The interval of thickness to be removed is configured as 50 μ m for the layers close to the surface and then gradually increases towards the center layer of the sample. After each polishing step, microscopic images of the sample surface are taken using a digital optical microscope (Keyence vhx2000).



(a)

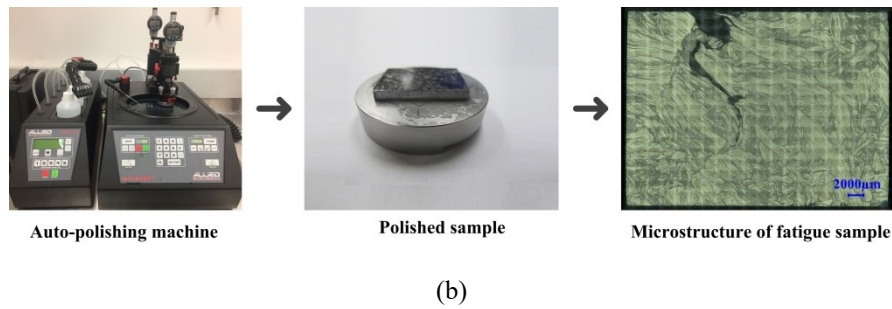


Figure 2. Experiments on SMC material for (a) strain distribution measurement with two DIC systems and (b) microstructure characterization by an automatic polishing system

3. Experimental results and discussion

3.1. Failure modes and fatigue performance

Twenty-five tests are performed under different loading levels for the long sample, while 5 additional tests are conducted under a medium loading level ($\Delta S=144\text{MPa}$) for the short sample. Typical failure modes are shown in Figure 3(a). Minor cracks are observed at a distance away from the location of the final fracture for several fatigue samples, which is similar to previous observations in quasi-static testing [10].

In the constant-amplitude fatigue test, the data are typically called $S-N$ data, reflecting the number of cycles N at the stress level S required to fail the sample. The $S-N$ data of all test results are plotted in Figure 3(b) using the stress range. It can be found that the average fatigue life of the long sample is much shorter than that of the short one under the same loading level, which indicates that the size effect may not be ignored in the durability modeling of the SMC composites. It is important to note that the nominal stress, which does not consider the local property variation, results in a very large scatter band in the $S-N$ diagram.

It is also worth mentioning that the collected temperature histories on the sample surface show that the temperature variation is not significant and that the maximum increment is approximately 6°C during fatigue testing.

$$UTS = aE_{average-failure} + b \quad (1)$$

Here $a=6.9E-3$ and $b=79\text{MPa}$ are calibrated material constants.

It is found that nearly 90% of tension-tension fatigue samples are broken at the area with relative low average modulus E_{RL} , e.g., sample S-1 shown in Figure 5(a). The E_{RL} is defined as below,

$$E_{RM} \leq E_{RL} \leq 1.1 * E_{RM} \quad (2)$$

where E_{RM} is the lowest average modulus within specimen. This phenomenon is reasonable owing to the correlation between local modulus and chip orientation distribution, which is demonstrated in previous work [10]. The areas with low $E_{average}$ tend to have more chips that align along the transverse direction to the loading direction, while areas with high $E_{average}$ tend to have chips more aligned along the loading direction. Since reinforcement of the carbon fiber chip is the most significant when the loading direction is along the chip direction, a positive correlation between fatigue strength and $E_{average}$ can be achieved. Further, the UTS of each sample is proposed to normalize the original FDP , the stress range. The new FDP is defined as,

$$FDP = \frac{\Delta S}{UTS} \quad (3)$$

The main trend of fatigue behavior is more distinct in Figure 5(b), and the correlation between the new FDP and fatigue life becomes much better with a larger correlation coefficient R-square value compared with the results in Figure 3(b). With considering the relationship between local modulus and microstructure, it can be concluded that the larger scatter in fatigue behavior of SMC composite is induced by the effect of chip orientation distribution. The fatigue behavior of SMC composite can be well described with $E_{average}$, which is determined by the chip orientation distribution. Note that the new FDP can also be useful for the size effect correction between the short and long samples, as the size effect on SMC composite is exactly determined by the possibility of low $E_{average}$.

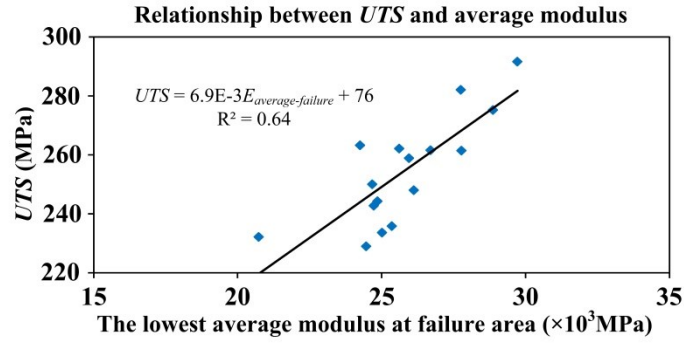
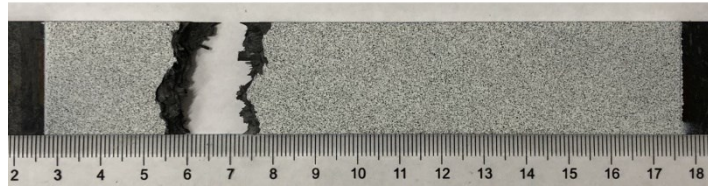
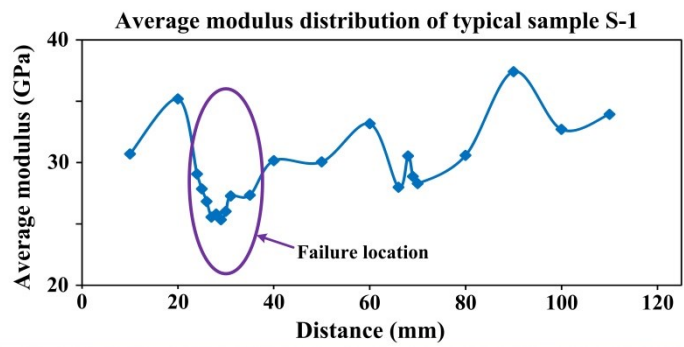
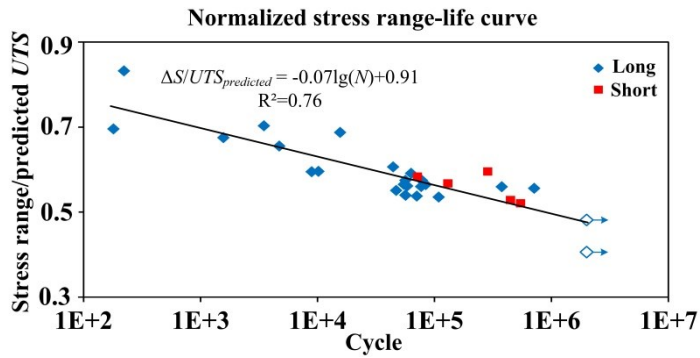


Figure 4. Relationship between *UTS* and the lowest average modulus at failure area



(a)



(b)

Figure 5. Fatigue behavior of SMC material for (a) average modulus distribution of one typical sample and the corresponding failure area and (b) relationship between fatigue life and stress range normalized by predicted *UTS*

3.3. Fatigue crack initiation and propagation for SMC materials

3.3.1. Crack initiation and initial propagation

Interrupted fatigue tests are carried out under a medium loading level ($\Delta S=144\text{MPa}$) with long samples. Fatigue experiments are suspended at the early stage, and the area with the lowest average modulus is cut off from the samples, as shown in Figure 6(a). Since there is a linkage between the failure area and relative low average modulus, layer-by-layer microstructure analysis on these samples cut from the local area with the lowest average modulus within sample would be helpful for understanding the crack initiation behavior of the SMC composite.

The lowest average modulus of one typical sample S-2 is 25.2GPa, and the corresponding predicted lives are about $6.5\text{E}+4$ cycles based on the normalized stress approach. The two samples are tested up to $1\text{E}+4$ cycles, and the modulus variation during this procedure is recorded with DIC systems. The degradation curves of the lowest average modulus are shown in Figure 6(b).

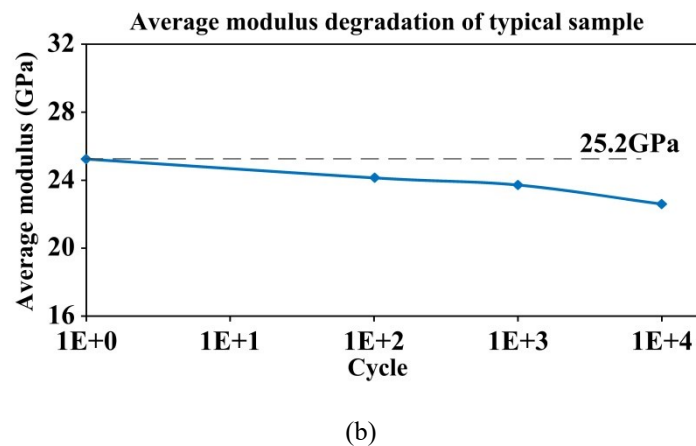
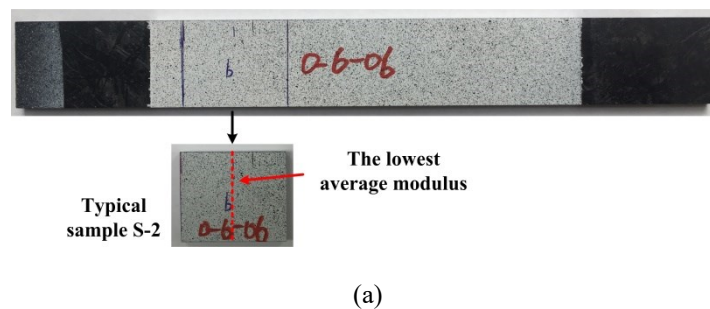


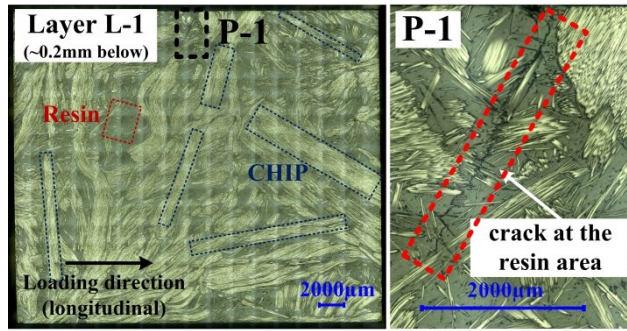
Figure 6. Interrupted fatigue samples for fatigue failure mechanism analysis for (a) typical samples S-2 for crack initiation analysis and (b) average modulus degradation of the sample

It can be found that the average modulus degradation may occur at the early stage of the fatigue test,

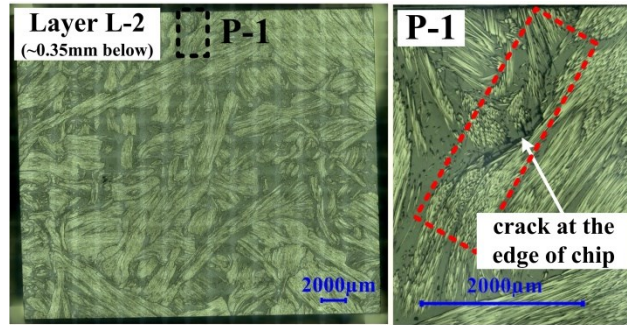
e.g., S-2. Layer-by-layer microstructure analysis can be helpful for understanding the mechanism of crack initiation. Among them, several significant layers will be discussed in detail here. For convenience, they are labeled from layer L-1 to L-6, which are approximately 0.2mm, 0.35mm, 1.1mm, 1.2mm, 2.2mm, and 2.3mm below the surface, respectively. In the following microscopic images, the chips are represented by white pixels while the resin is represented by the grey ones.

In layer L-1 and L-2, as shown in Figure 7(a) and (b), which are close to the surface, only a small crack close to the transverse direction occurs at the resin area as well as at the edge of a chip, and it propagates among adjacent layers. Note that cracks are confirmed by the microstructure comparison between the different layers. As the diameter of a single fiber is only about $7\mu\text{m}$, this approach is efficient for eliminating the confusion of fibers dropping off. In layers L-3 and L-4 in Figure 7(c) and (d), the crack cannot be observed anymore, and also no other cracks occur at these layers. In layers L-5 and L-6, as given in Figure 7(e) and (f), which are near the center of the polished samples, several independent cracks initiate. In particular, three typical independent locations with cracks, namely A-C, are presented here. At location A, a crack close to the transverse direction appears at the resin area and inside a chip. At location B, transverse cracks occur inside chips, at the resin areas, and at the edges of chips. At location C, two cracks close to the transverse direction are observed inside chips.

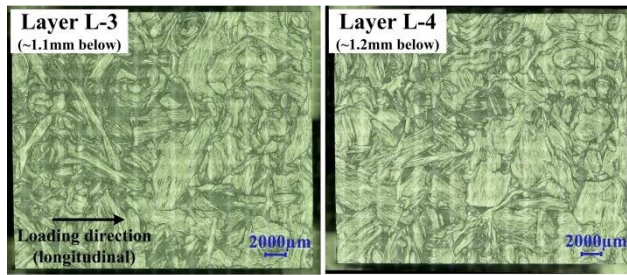
In summary, at the early stage of the fatigue test for SMC materials, cracks along or close to the transverse direction initiate not only at different locations but also at different layers simultaneously. Generally, cracks are at the edge of chips and inside chips as well as at the resin area. Chip breakage is not observed in this processing. It also should be mentioned that the orientation of chips in the area with these initial cracks is mainly along transverse direction. Since the areas with low $E_{average}$ tend to have more chips that align along the transverse direction, the fatigue failure occurs much earlier at the low $E_{average}$ area, which agrees with the above-mentioned fatigue results.



(a)

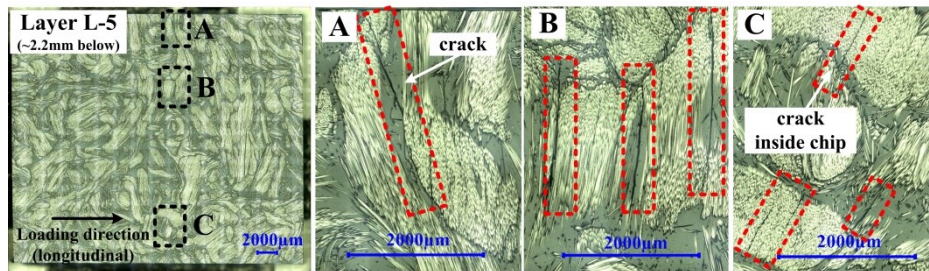


(b)

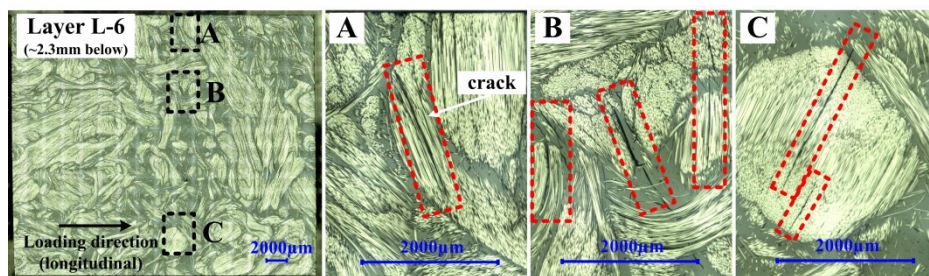


(c)

(d)



(e)



(f)

Figure 7. Typical layers in sample S-2 for (a) layer L-1, (b) layer L-2, (c) layer L-3, (d) layer L-4, (e) layer L-5, and (f) layer L-6

3.3.2. Crack propagation

By comparison, several interrupted fatigue experiments are stopped prior to final failure to analyze the crack propagation in detail, and major cracks are already very obvious, e.g., typical sample S-3 in Figure 8(a). Based on data analysis of the failure samples, the increment of displacement range $D_{\text{Increment}}$ for the long sample is not significant before final failure and increases dramatically to approximately 0.1mm at the end of the fatigue tests, as shown in Figure 8(b). Here, N/N_f is the cycle divided by the fatigue life. It should be mentioned that the evolution of the average modulus is not measured for each cycle. In order to capture the condition just prior to final failure, the increment of displacement range is monitored and chosen as the failure indicator roughly for convenience. Sample S-3 is loaded for $3.8E+5$ cycles under the stress range of 144MPa. At the end of the interrupted fatigue test, the increment of displacement range is 0.073mm, which is also plotted in Figure 8(b). It is believed that sample S-3 is just prior to final failure.

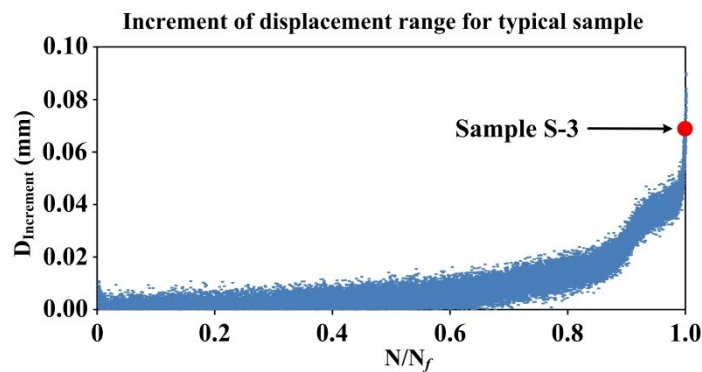
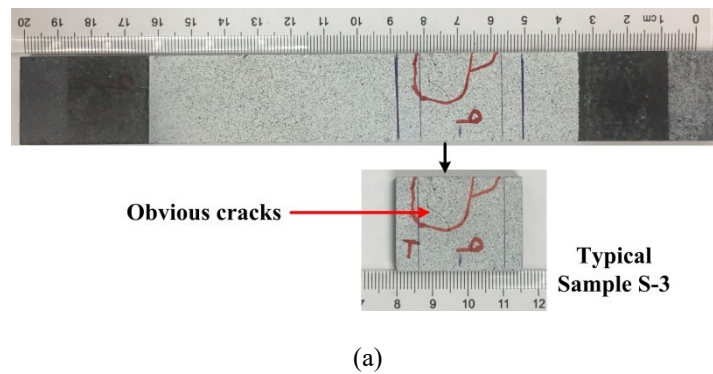


Figure 8. Interrupted fatigue sample for fatigue failure mechanism analysis for (a) typical sample S-3 for crack propagation analysis and (b) increment of displacement range for one typical sample and the corresponding condition of sample S-3

Similarly, it is further polished to study the crack propagation of SMC materials during the fatigue test. Representative layers labeled as layer L-7, L-8, and L-9, which are about 0.2mm, 1.2mm and 2.2mm below the surface, respectively, will be discussed.

In layer L-7 (Figure 9(a)), a major crack has already formed by crack bridging. Due to delamination, some chips are dropped out during polishing. In layer L-8 (Figure 9(b)), even as obvious cracks appear at two sides of the chips, chip breakage still cannot be observed in propagation processing. In layer L-9 (Figure 9(c)), a major crack has bridged together from upper to bottom, and no chip breakage occurs. Therefore, chip breakage is not the main failure form during SMC fatigue experiments.

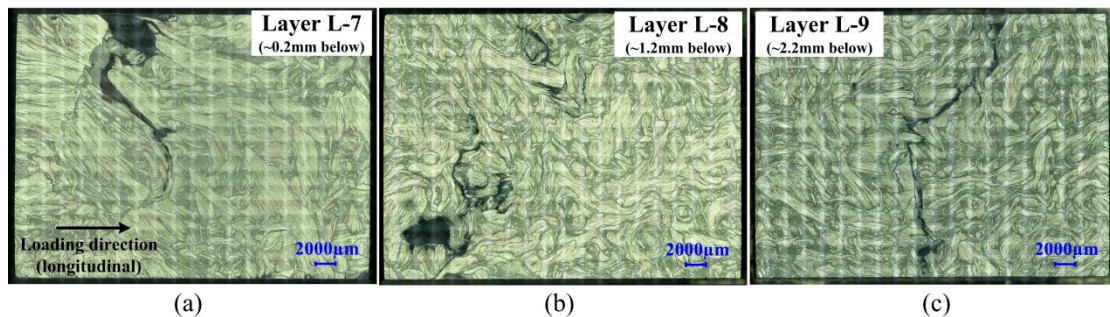


Figure 9. Representative layers in sample S-3 for (a) layer L-7, (b) layer L-8, and (c) layer L-9

4. Numerical Modeling

The chip-packing-based representative volume element (RVE) model [20] has proved to be a good approach to predict the mechanical response of an SMC composite with geometries and material properties of SMC meso-structures. In this section, a new reconstruction approach is introduced, and then the general framework of an RVE-based fatigue damage model is discussed.

4.1. Reconstruction algorithm

The stochastic chip packing reconstruction algorithm has been established in the RVE modeling of SMC composites, and a good agreement has been achieved between numerical predictions and experiments in the stiffness analysis [20]. In a single layer, this reconstruction procedure creates the chip by assigning a set of separate voxels to the corresponding area. Between adjacent layers, a chip

segment reallocation process, called the “rise and sink” process, is introduced to move voxels to the upper and lower layers to reproduce curved chips and also to increase the space utilization. However, such a voxel-based reconstruction algorithm and “rise and sink” process will result in zigzags at the edge of chips and holes inside of chips, as shown in Figure 10, which is not suitable for fracture and fatigue analysis [22].

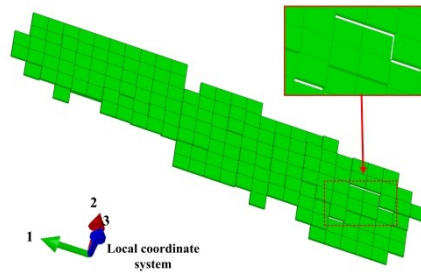


Figure 10. One representative chip in the stochastic chip packing reconstruction model

On the basis of the chip packing reconstruction algorithm [20], a modified model is proposed in this section with consideration of the structure characteristics of SMC materials. Due to the influence of mixture processing during chip preparation as well as the effects of high temperature and high pressure in molding processing, fragments are always observed on the polished surface, and the chips inside SMC materials are deformed, as shown in a typical microstructure image of SMC materials (Figure 11(a)). Thus, chips with variable geometry are required in chip packing reconstructions. In this new reconstruction model, the length of the chip is generated randomly in a specific range. Then, for a given length, 12 control points P_1 - P_{12} are assigned along the edge of the original rectangular chip with the maximum width (Figure 11(b)). These 12 points will be adjusted randomly along the corresponding red line within a specific range based on the observed geometry characteristics. Additionally, in order to mimic the structure of chips inside the SMC materials, the fragments, the size of which is much smaller than that of the chip, are introduced during the final fine-tuning procedure.

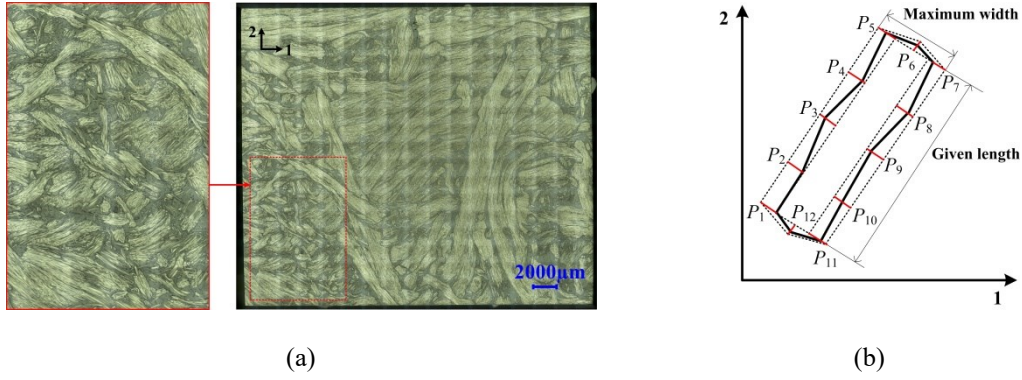


Figure 11. SMC reconstruction work for (a) a typical microstructure image of SMC materials and (b) variable geometry of chip inside SMC materials in reconstruction model

The inputs of this RVE model include the geometrical parameters of the chips, the target chip orientation tensor, and the target chip volume fraction. The thickness of the plaque is usually much smaller than the length of the chips in the SMC composites, which constrains the tendency of the chips to align along the out-of-plane direction. Thus, the planar chip orientation tensor [23] is sufficient to describe the chip orientation distribution for SMC composites. The outputs are the spatial coordinates of the chips and the corresponding orientations. In this algorithm, chip orientation sets are firstly generated by sampling the recovered chip orientation PDF [23], and the corresponding chip geometry sets are obtained according to the geometrical parameters of the chips in the pre-processing step. Next, chips are packed one-by-one and layer-by-layer under a modified random sequential adsorption (RSA) scheme until the chip volume fraction is close to the target. To avoid the zigzags in previous chip packing reconstruction models [20], this reconstruction is based on the geometry information of packing chips instead of separate voxels. The packing chip would be cut into several continuum parts and located at two adjacent layers on account of overlapping. Due to the high volume fraction at lower layers, only the “rise” process is needed for the modified RSA scheme. Finally, fine tuning is performed with small fragments to achieve the target chip orientation tensor and the target chip volume fraction. Then, the reconstructed structure is exported to ABAQUS for analysis. The detailed flow chart is plotted in Figure 12.

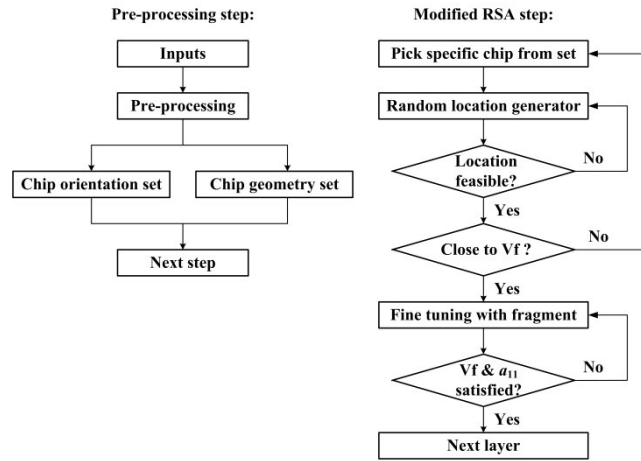


Figure 12. Flow chart for modified reconstruction model

4.2. RVE-based fatigue damage model

In order to study the fatigue characteristics of SMC materials at the macro-scale level accurately, a multi-scale fatigue model is proposed in the present work based on a modified reconstruction RVE model. There are five major steps in this workflow (Figure 13):

(1) The RVE model is established based on the above reconstruction algorithm as discussed in Section 4.1, and the values for the cycle of RVE model N and the damage parameter of all elements D are set to 0.

(2) An explicit analysis is carried out in ABAQUS on the SMC constitutive model, and the stress and strain state is determined for all elements involved in the RVE model.

(3) Check if the model is separated; if no, then go to (4), otherwise the simulation is completed.

(4) Different failure criteria of chip, resin, and interface are employed for corresponding elements, and the fatigue failure evolution is evaluated by the corresponding continuum damage models. The increment of cycles ΔN is calculated based on the weakest elements, which is determined by the stress state. In a single iteration, we do not update the stress and strain of the element when running the continuum damage model. Then, the cycle N of the RVE model is updated, i.e., $N_{i+1} = N_i + \Delta N$. Meanwhile, the damage parameter D for each element is accumulated respectively, i.e., $D_{i+1} = D_i + \Delta D$. When D reaches 1, the corresponding elements are completely damaged and deleted.

(5) The RVE model is rebuilt. Then, check if the new model works; if yes, then go to (2), otherwise the simulation is completed.

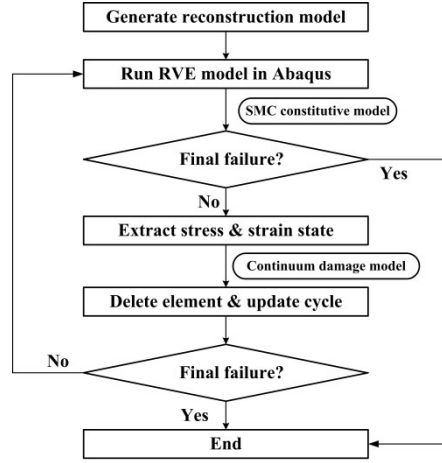


Figure 13. Flow chart for multi-scale fatigue model

The failure of chip, resin, and interface is numerically integrated using the continuum damage law in the proposed multi-scale fatigue damage model. Generally, the rate of damage evolution may be assumed as a power law function of the local stress [24-26]:

$$\frac{dD}{dN} = m_1 \left(\frac{\Delta\sigma}{S_{failure}} \right)^{m_2} \quad (4)$$

where D represents the damage parameter, N is the number of cycles, and m_1 and m_2 are material constants fitted based on the fatigue experiments. $\Delta\sigma$ is the localized stress range and can be material or failure-mode dependent. $S_{failure}$ is the failure strength. According to the failure mechanism of different phases in SMC composite, which is observed in the microstructure analysis, the damage law for chip, resin, and interface is developed respectively as below:

Chip

During fatigue testing of SMC materials, chip failure is found to be driven by chip splitting instead of chip breakage, and therefore the stress component perpendicular to the chip direction σ_{22} is selected in the damage model for the chip element. The coefficients m_1 and m_2 of the chip element can be calibrated with fatigue data of uni-directional fiber-reinforced composites (UD) along the transverse direction. Nevertheless, due to the in-situ effect [27, 28], the failure strength of chip $S_{chip-failure}$ in SMC materials should be superior to that of UD along the transverse direction. The continuum damage model of the chip element is written as:

$$\frac{dD}{dN} = m_1 \left(\frac{\Delta\sigma_{22}}{S_{chip-failure}} \right)^{m_2} \quad (5)$$

where $\Delta\sigma_{22}$ is a variable, and the σ_{22} at different stages can be extracted during numerical simulation.

Resin

Due to the complex stress state of resin, von Mises stress σ_{mises} is used in the damage law of the resin element. As the fatigue failure of UD along the transverse direction is matrix-dominated [29], the fatigue behavior of the resin should be close to that of UD along the transverse direction; the coefficients m_1 and m_2 of the resin element follow those in the chip element. $S_{resin-failure}$ refers to the failure strength of resin in SMC materials. Then, the continuum damage law of the resin element is expressed as:

$$\frac{dD}{dN} = m_1 \left(\frac{\Delta\sigma_{mises}}{S_{resin-failure}} \right)^{m_2} \quad (6)$$

$$\sigma_{mises} = \sqrt{\frac{(\sigma_{11} - \sigma_{22})^2 + (\sigma_{22} - \sigma_{33})^2 + (\sigma_{33} - \sigma_{11})^2 + 6(\sigma_{12}^2 + \sigma_{23}^2 + \sigma_{31}^2)}{2}}$$

where $\Delta\sigma_{mises}$ is a variable, and the σ_{mises} at different stages can be extracted during numerical simulation.

Interface

The interface fracture is assumed to be determined by the opening stress and shear stresses. Then, the most significant one among model I, II, and III would be used in the continuum damage model for the interface element. Technically, the coefficients m_1 and m_2 of the interface element should be calibrated based on the fatigue result of the interface. However, due to the lack of the relevant experimental data, the coefficients m_1 and m_2 of the interface element is assumed to be close to that of the resin in the present study. $S_{interface-failure}$ refers to the failure strength of the interface in SMC material. The continuum damage law of the cohesive element can be given as,

$$\frac{dD}{dN} = m_1 \left(\frac{\max(\Delta\sigma_{33}, \Delta\sigma_{13}, \Delta\sigma_{23})}{S_{interface-failure}} \right)^{m_2} \quad (7)$$

where $\Delta\sigma_{33}$, $\Delta\sigma_{13}$, $\Delta\sigma_{23}$ are variables, and the σ_{33} , σ_{13} , σ_{23} at different stages can be extracted during numerical simulation.

5. Simulation results and discussions

5.1. Reconstruction of meso-structures

The proposed reconstruction algorithm is applied to reproduce the meso-structures of the SMC materials. Due to the various chip distributions in SMC materials, eight representative cases with four different chip distributions are generated using the parameters in Table 1. The typical layers of different chip distributions are plotted in Figure 14(a).

Table 1. Pre-specified Input Parameters

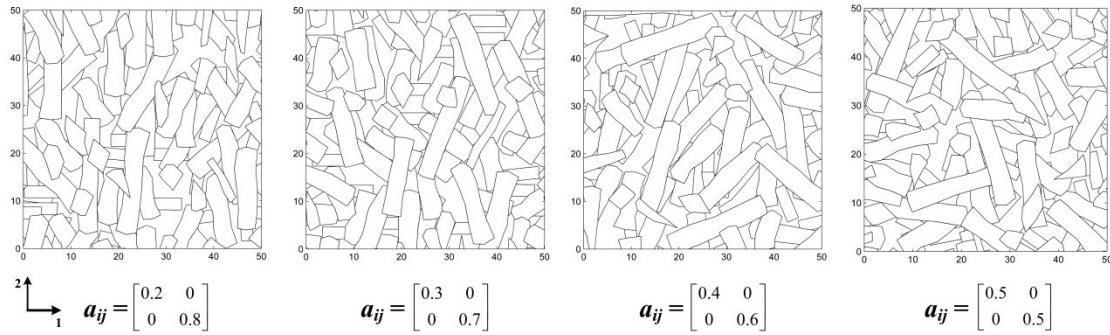
Name	Value
RVE size	50 mm × 50 mm × 0.8mm
Layers	8
Chip volume fraction	80%
Chip size	(15~25) mm × (2~5) mm × 0.1 mm
Chip orientation tensor	$\begin{bmatrix} 0.2 & 0 \\ 0 & 0.8 \end{bmatrix}, \begin{bmatrix} 0.3 & 0 \\ 0 & 0.7 \end{bmatrix}, \begin{bmatrix} 0.4 & 0 \\ 0 & 0.6 \end{bmatrix}, \begin{bmatrix} 0.5 & 0 \\ 0 & 0.5 \end{bmatrix}$

In the RVE model, elements associated with chips, resin, and interface are assigned with the corresponding material properties [21, 30], as listed in Table 2. The cohesive element is introduced to describe the interface between chip and resin as well as that between chips. The homogeneous traction boundary conditions are added in the finite element analysis (FEA), which coincides with the loading in fatigue tests (Figure 14(b)). The freedom of the X direction for surface 1, the Z direction for surface 2, the Y direction for surface 5 is fixed to eliminate the rigid body movement of the RVE model, as shown in Figure 14(b). The nodes on surface 4 are coupled to the reference node RN. The load is applied on the reference node RN along X direction. It has been proved that for sufficiently large RVEs, the results obtained from models with such boundary conditions are close to those obtained from using periodic boundary condition (PBC) [31-33]. A typical stress contour under in-plane uniaxial load is illustrated in Figure 14(c).

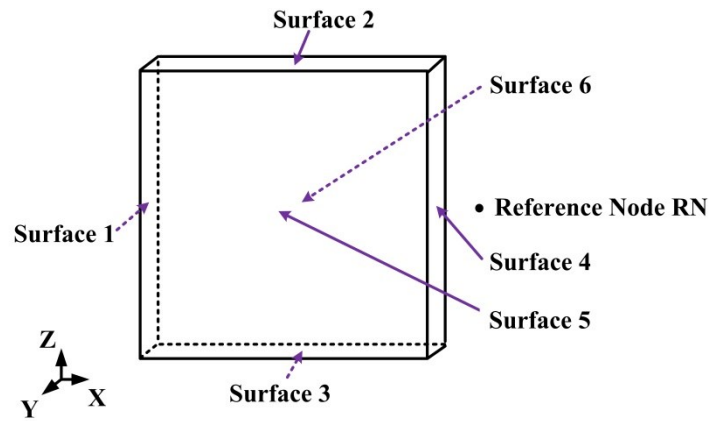
Table 2. Chip, resin and interface properties

Chip (transversely isotropic)	Resin (isotropic)	Interface
-------------------------------	-------------------	-----------

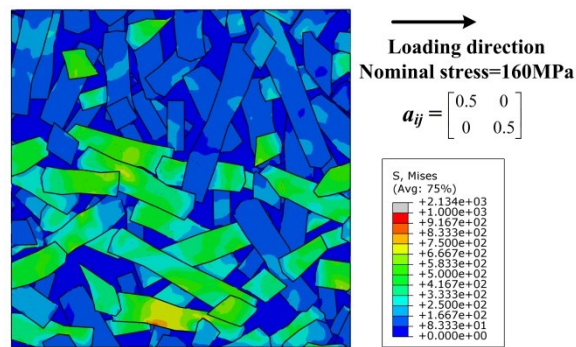
E_{11} (GPa)	125.9	μ_{12}	0.32	E (GPa)	3.3	K (GPa/mm)	30
E_{22} (GPa)	8.6	μ_{23}	0.61	μ	0.38	ρ (ton/mm ³)	1.26E-09
G_{12} (GPa)	4.8	ρ (ton/mm ³)	1.53E-09	ρ (ton/mm ³)	1.26E-09		



(a)



(b)



(c)

Figure 14. Reconstruction results of SMC material for (a) representative layers for different chip distributions, (b) boundary conditions for simulation, and (c) a typical stress contour of established

FEA models

5.2. Fatigue life predictions

In this section, the fatigue behavior of the SMC materials is investigated based on the proposed RVE-based fatigue damage model. Follow-up fatigue analysis will be conducted on the eight RVE models built in section 5.1.

All parameters are summarized in Table 3. The material constants m_1 and m_2 in the damage law are fitted based on the fatigue data ($R=0.1$) of UD along the transverse direction, as shown in Figure 15 [34]. $S_{chip-failure}$ is calculated based on the theory for in-situ strengths of thin embedded plies in Ref. [28]. $S_{resin-failure}$ is from the experimental data of pure resin. $S_{interface-failure}$ is set as 57MPa [35, 36].

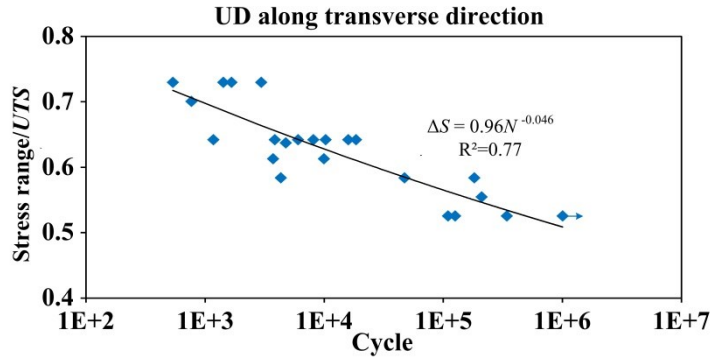


Figure 15. S - N fatigue diagram of UD along transverse direction

Table 3. Coefficients in multi-scale fatigue model

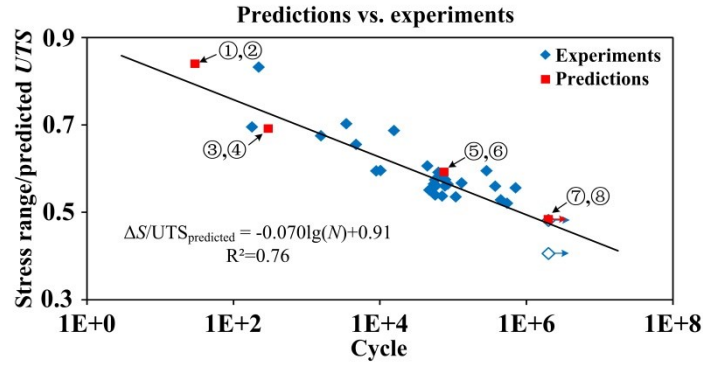
Coefficient	Value
m_1	2.67
m_2	21.74
$S_{chip-failure}$	242MPa
$S_{resin-failure}$	85MPa
$S_{interface-failure}$	57MPa

According to the modified RSA algorithm, the chip distribution in RVEs should be close to a uniform condition. Without considering the small variation of chip distribution in RVEs, the average modulus can be obtained based on the relationship between the chip orientation tensor and the stiffness matrix in Ref. [20], and UTS can be estimated by Eq. (1). In order to highlight the effect of chip orientation distribution, the same fatigue loading is set for the eight RVE models with different chip orientation

tensors, which are labeled from 1 to 8. The maximum nominal stress is 160MPa and the load ratio is 0.1. The predicted fatigue results are normalized by the *UTS* and plotted in Figure 16(a) with the experimental data for comparison. While the component in chip orientation tensor a_{11} equals to 0.2, the chips are mostly aligning along directions transverse to the loading direction. In this case the average modulus is very low, and the corresponding life is shortest. While a_{11} equals to 0.5, the chip orientation distribution is a random condition. Then, the average modulus calculated is highest among the eight cases, and the predicted life is also the longest. The effect of chip orientation distribution on fatigue behavior of SMC composite is well captured in the present work. In particular, the correlation between experimental and predicted fatigue results is very good.

A typical fatigue damage progress during cyclic loading is illustrated in Figure 16(b), for which the a_{11} equals to 0.3. Cracks are observed at the edge of chips and inside chips as well as at the resin area. Meanwhile, chip breakage is not the main failure form before final failure. As shown in image of the 100th cycle, cracks occur at different locations without bridging together, which is similar as the experimental failure evolution of SMC composite. Different fatigue failure modes are successfully reproduced in numerical simulation, which are marked as shown in Figure 16(b) for comparison.

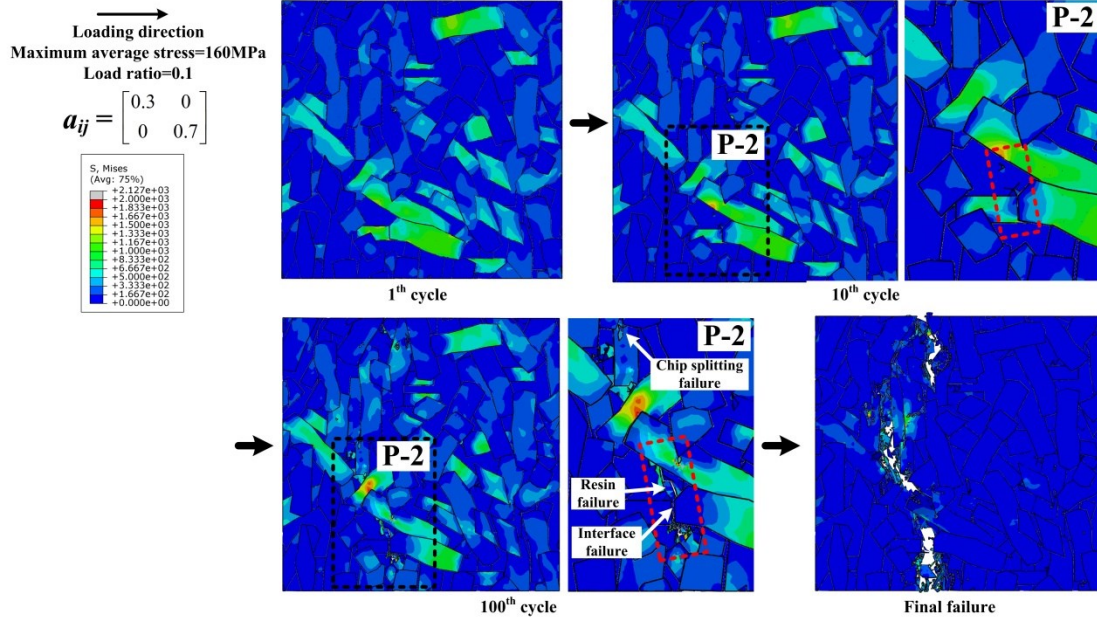
The good correlation between predicted and experimentally measured fatigue life and failure modes indicates that the proposed methodology, including a modified reconstruction approach and the RVE-based fatigue damage model, is suitable for prediction of the fatigue life of SMC materials under uniaxial loading conditions. It is important to note that the current modelling technique offers a novel approach to determine the constant fatigue life diagram associated with different failure modes of SMC materials by means of a multi-scale fatigue model, and it should be able to be extended to other loading conditions.



$$a_{ij} = \begin{bmatrix} 0.2 & 0 \\ 0 & 0.8 \end{bmatrix} : \textcircled{1}, \textcircled{2} \quad a_{ij} = \begin{bmatrix} 0.3 & 0 \\ 0 & 0.7 \end{bmatrix} : \textcircled{3}, \textcircled{4}$$

$$a_{ij} = \begin{bmatrix} 0.4 & 0 \\ 0 & 0.6 \end{bmatrix} : \textcircled{5}, \textcircled{6} \quad a_{ij} = \begin{bmatrix} 0.5 & 0 \\ 0 & 0.5 \end{bmatrix} : \textcircled{7}, \textcircled{8}$$

(a)



(b)

Figure 16. Fatigue simulation results for SMC materials for (a) predictions of eight typical reconstructions vs. experimental data of SMC materials and (b) stress contour of one typical case under maximum stress condition after different cycles

6. Conclusions

The fatigue crack initiation and fracture behavior of compression-molded SMC composed of chopped carbon fiber chip-reinforced composites under tension-tension loading condition have been experimentally and numerically investigated. Large scatter in the $S-N$ diagram is observed due to the

variation in chip distribution among coupons.

A new method is proposed to describe the fatigue behavior of chopped carbon fiber chip-reinforced composites accurately based on microstructure characteristics. Heterogeneous modulus distribution is observed, and samples fail at the local area with a relative low average modulus during tension-tension loading conditions. A better correlation is achieved in the *S-N* diagram by normalizing the applied stress range with the estimated *UTS* from the lowest average modulus at the failure area.

Interrupted fatigue tests are also performed to investigate fatigue crack initiation and propagation. The microstructure shows that cracks along or close to the transverse direction initiate in the resin areas and at the edge of chips as well as inside chips at the early stage. In addition, no obvious chip breakage can be observed even just prior to the final failure.

Finally, a multi-scale progressive damage fatigue model is proposed by incorporating a modified stochastic algorithm for 3D chip packaging reconstruction along with continuum damage models into the RVE model in ABAQUS/Explicit. The results of the model are in good agreement with the experimental data in terms of cracking modes and predicted life.

Acknowledgements

This research is supported by Ford Motor Company with funding from the U.S. Department of Energy's Office of Energy Efficiency and Renewable Energy (EERE) under Award Number DE-EE0006867. A supercomputing grant from HPC System at Ford Motor Company is acknowledged. The authors also gratefully acknowledge the contribution of Dr. Guanhan Wu for the detailed discussion of this work.

Reference

- [1] Feraboli P., Peitso E., Cleveland T. Modulus measurement for prepreg-based discontinuous carbon fiber/epoxy systems. *J Compos Mater.* 2009;43. 1947-1965.
- [2] Mechakra M., Nour A., Lecheb S., Chellil A. Mechanical characterizations of composite material with short Alfa fibers reinforcement. *Compos Struct.* 2015;124. 152-162.
- [3] Neiri M., Notta-Cuvier D., Lauro F., Chaari F., Maalej Y., Zouari B. Modelling and characterisation of dynamic behaviour of short-fibre-reinforced composites. *Compos Struct.* 2017;160. 516-528.
- [4] Sun W., Vassilopoulos A.P., Keller T. Experimental investigation of kink initiation and kink band

- formation in unidirectional glass fiber-reinforced polymer specimens. *Compos Struct.* 2015;19. 9-17.
- [5] Ma Y., Ueda M., Yokozeki T., Sugahara T., Yang Y., Hamada H. A comparative study of the mechanical properties and failure behavior of carbon fiber/epoxy and carbon fiber/polyamide 6 unidirectional composites. *Compos Struct.* 2017;160. 89-99.
- [6] Feraboli P., Peitso E., Deleo L., Cleveland T. Characterization of prepreg-based discontinuous carbon fiber/epoxy systems. *J Reinf Plast Compos* 2009;28. 1191-1214.
- [7] Feraboli P., Peitso E., Cleveland T., Stickler P.B., Halpin J.C. Notched behavior of prepreg-based discontinuous carbon fiber/epoxy systems. *Compos Part A-Appl S.* 2009;40. 289-299.
- [8] Febraboli P., Cleveland T., Stickler P., Halpin J. Stochastic laminate analogy for simulating the variability in modulus of discontinuous composite materials. *Compos Part A-Appl S.* 2010;41. 557-570.
- [9] Johanson K., Harper L.T., Johnson M.S., Warrior N.A. Heterogeneity of discontinuous carbon fibre composites: damage initiation captured by digital image correlation. *Compos Part A-Appl S.* 2015;68. 304-312.
- [10] Tang H.B., Chen Z.X., Zhou G.W., Li Y., Avery K., Guo H.D., Kang H., Zeng D., Su X.M. Correlation between failure and local material property in chopped carbon fiber chip-reinforced sheet molding compound composites under tensile load. *Polym Composite.* 2018. (Online)
- [11] Selezneva M., Lessard L. Characterization of mechanical properties of randomly oriented strand thermoplastic composites. *J Compos Mater.* 2016;50. 2833-2851.
- [12] Horst J.J., Spoomaker J.L. Mechanisms of fatigue in short glass fiber reinforced polyamide 6. *Polymer Engineering and Science.* 1996;36. 2718-2726.
- [13] Horst J.J., Spoomaker J.L. Fatigue fracture mechanisms and fractography of short-glassfibre-reinforced polyamide 6. *Journal of Materials Science.* 1997;32. 3641-3651.
- [14] Tanaka K., Kitano T., Egami N. Effect of fiber orientation on fatigue crack propagation in short-fiber reinforced plastics. *Engineering Fracture Mechanics.* 2014;123. 44-58.
- [15] De Monte M., Moosbrugger E., Quaresimin M. Influence of temperature and thickness on the off-axis behaviour of short glass fibre reinforced polyamide 6.6 - quasi-static loading. *Compos Part A-Appl S.* 2010;41. 859-871.
- [16] De Monte M., Moosbrugger E., Quaresimin M. Influence of temperature and thickness on the off-axis behaviour of short glass fibre reinforced polyamide 6.6 - cyclic loading. *Compos Part A-Appl S.* 2010;41. 1368-1379.

- [17] De Monte M., Moosbrugger E., Quaresimin M. Multiaxial fatigue of a short glass fibre reinforced polyamide 6.6 - fatigue and fracture behaviour. *Int J Fatigue*. 2010;32. 17-28.
- [18] Li Y., Chen Z., Xu H., Dahl J., Zeng D., Mirdamadi M., Su X. Modeling and Simulation of Compression Molding Process for Sheet Molding Compound (SMC) of Chopped Carbon Fiber Composites. *SAE Int J Mater Manf*. 2017;10. 130-137.
- [19] ASTM D3479/D3479M-12. Tension-tension fatigue of polymer matrix composite materials.
- [20] Chen Z.X., Huang T.Y., Shao Y.M., Li Y., Xu H.Y., Avery K., Zeng D., Chen W., Su X.M. Multiscale Finite Element Modeling of Sheet Molding Compound (SMC) Composite Structure based on Stochastic Mesostructure Reconstruction. *Compos Struct*. 2018;188. 25-38.
- [21] Li Y., Chen Z.X., Su L.X., Chen W., Jin X.J., Xu H.Y. Stochastic Reconstruction and Microstructure Modeling of SMC Chopped Fiber Composites. *Compos Struct*. 2018;200. 153-164.
- [22] Doitrand A., Fagiano C. Irisarri F.X. Hirsekorn M. Comparison between voxel and consistent meso-scale models of woven composites. *Compos Part A-Appl S*. 2015;73. 143-154.
- [23] Advani S.G., Tucker C.L. The use of tensors to describe and predict fiber orientation in short fiber composites. *J Rheol*. 1987;31. 751-784.
- [24] Mao H., Mahadevan S. Fatigue damage modelling of composite materials. *Compos Struct*. 2002;58. 405-410.
- [25] Shenoy V., Ashcroft L.A., Critchlow G.W. Crocombe A.D. Unified methodology for the prediction of the fatigue behaviour of adhesively bonded joints. *Int J Fatigue*. 2010;32. 1278-1288.
- [26] Solana A.G. Crocombe A.D., Ashcroft I.A. Fatigue life and backface strain predictions in adhesively bonded joints. *Int J Adhes Adhes*. 2010;30. 36-42.
- [27] Parvizi A., Garrett K., Bailey J. Constrained cracking in glass fibre-reinforced epoxy cross-ply laminates. *J Mater Sci*. 1978;13. 195-201.
- [28] Pinho S.T. Modelling failure of laminated composites using physically-based failure models. University of London. 2005.
- [29] Hashin Z., Rotem A. A fatigue failure criterion for fiber reinforced materials. *J Compos Mater*. 1973;7. 448-464.
- [30] Turon A., Davila C.G., Camanho P.P., Costa J. An Engineering Solution for using Coarse Meshes in the Simulation of Delamination With Cohesive Zone Models. NASA/TM-2005-213547. 2005.
- [31] Kanit T., Forest S., Galliet I., Mounoury V., Jeulin D. Determination of the size of the

representative volume element for random composites: statistical and numerical approach. *Int J Solids Struct.* 2003;40. 3647-3679.

[32] Pahr D., Böhm H. Assessment of mixed uniform boundary conditions for predicting the mechanical behavior of elastic and inelastic discontinuously reinforced composites. *Comp Model Eng.* 2008;34. 117-136.

[33] Chen G., Ozden U., Bezold A., Broeckmann C. A statistics based numerical investigation on the prediction of elasto-plastic behavior of WC-Co hard metal. *Comp Mater Sci.* 2013;80. 96-103.

[34] Liu H.L., Avinesh O., Li Z.A., Carlos E.P., Su X.M. Size effect on the fatigue behavior of carbon fiber/epoxy laminated composites. *Compos Struct.* (Under review)

[35] Vaughan T.J., McCarthy C.T. Micromechanical modelling of the transverse damage behaviour in fibre reinforced composites. *Compos Sci Technol.* 2011;71. 388-396.

[36] Melro A.R., Camanho P.P., Andrade Pires F.M., Pinho S.T. Micromechanical analysis of polymer composites reinforced by unidirectional fibres: Part II – Micromechanical analyses. *Int J Solids Struct.* 2013;50. 1906-1915.